Chaos, Solitons and Fractals 145 (2021) 110802

Contents lists available at ScienceDirect

Chaos, Solitons and Fractals

Nonlinear Science, and Nonequilibrium and Complex Phenomena

journal homepage: www.elsevier.com/locate/chaos

Frontiers

Fractal and multifractal analysis of electrochemical noise to corrosion evaluation in A36 steel and AISI 304 stainless steel exposed to MEA-CO_2 aqueous solutions

Mariana Ramírez-Platas, Miguel A. Morales-Cabrera, Victor M. Rivera, Epifanio Morales-Zarate, Eliseo Hernandez-Martinez*

Facultad de Ciencias Químicas, Universidad Veracruzana, Xalapa Veracruz, México

ARTICLE INFO

Article history:
Received 11 November 2020
Revised 24 January 2021
Accepted 17 February 2021
Available online 2 March 2021

Keywords:
R/S analysis
Corrosion evaluation
CO_2 capture

ABSTRACT

In this work, a proposal based on the fractal and multifractal analysis of electrochemical noise (EN) to corrosion evaluation in A36 steel and AISI 304 stainless steel, exposed in aqueous solutions of monoethanolamine (MEA) with carbon dioxide (CO_2), is presented. Time-series of potential and current captured during the corrosion process of both steels exposed to different conditions of temperature and MEA concentration were analyzed using the rescaled range (R/S) method. The R/S analysis identified three characteristic regions that suggest that the time-series contain information associated with different physical phenomena in the corrosion process, that could be related to transport mechanisms and chemical reactions. The Hurst exponents calculated allow identifying correlations associated with the type and degree of corrosion, as well as information on the corrosion mechanisms of both steels evaluated. Hence, the Hurst exponent calculated from potential and current time-series could be used as an inexpensive and easily implemented tool for rapid diagnosis of the corrosive effects in the steel equipment used in the absorption processes of CO_2 capture with amines.

1. Introduction

Carbone dioxide (CO_2) capture by chemical absorption using aqueous monoethanolamine (MEA) solutions is one of the most widely used technologies in the chemical industry, since the process is thermally stable, selective and achieves efficiencies greater than 90% absorption. However, it presents difficulties such as the corrosion of the operating equipment, which requires the implementation of maintenance strategies to increase the useful life of the equipment and avoid accidents [1,2]. Corrosion is a complex process that contemplates the interaction between transport processes and chemical reactions, so that in order to implement diagnostic mechanisms of the type and degree of corrosion it is necessary to know the factors involved in the process, for example, the physicochemical characteristics of solution (aqueous or gaseous), properties of the equipment material, conditions of the experimental system such as temperature, pressure, oxygen concentration, among others. In this sense, specific studies have been reported on the effect of such variables in the degree and type of corrosion of reactive CO_2 absorption. For example, Kittel et al. [3] evaluated the degree of corrosion of AISI 1018 (carbon steel) and AISI 304 (stainless steel) exposed in MEA-CO_2 solutions, using weight loss coupons installed at six different locations in absorption columns. Their results showed that the temperature and CO_2 concentration have a direct effect on the degree of corrosion, finding that corrosion is favored in the areas of the equipment with the highest temperature and it increases when operating with high CO_2 loads. Kittel et al. [4] analyzed the corrosion of carbon steel in two processes, natural gas processing and CO_2 capture, at different operating conditions. For a constant CO_2 load, they found that the corrosion rate increases with increasing temperature, while the monoethanolamine (MEA) concentration is not a determining factor under the conditions studied. On the other hand, Xiang et al. [5] evaluated the corrosion of A36 carbon steel in 30% MEA solutions, using electrochemical techniques and weight loss methods at different operating conditions. Their results showed that the increase in O_2 flow and temperature increases the corrosion rate. Erfani et al. [6] determined corrosion in carbon and stainless steel with variations in temperature and MEA concentration, using the linear polarization resistance method, weight loss coupons, and

* Corresponding author.
E-mail addresses: elisehernandez@uv.mx, elijazfan@yahoo.com (E. Hernandez-Martinez).

https://doi.org/10.1016/j.chaos.2021.110802
0960-0779/

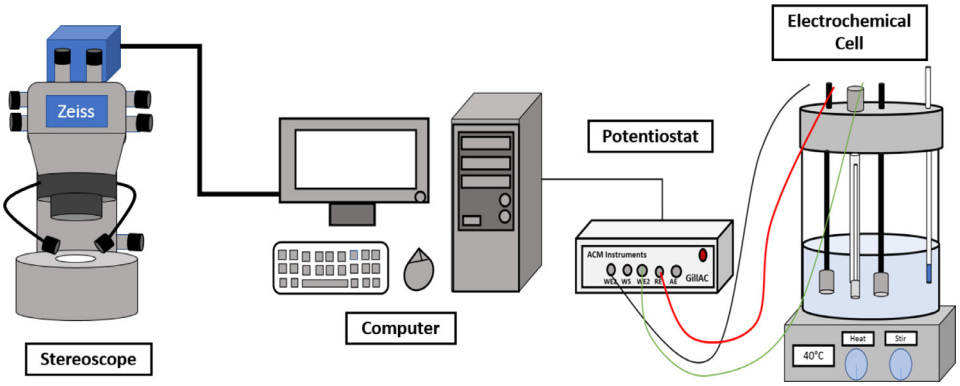

Fig. 1. Experimental set-up of potentiostat and data acquisition system.

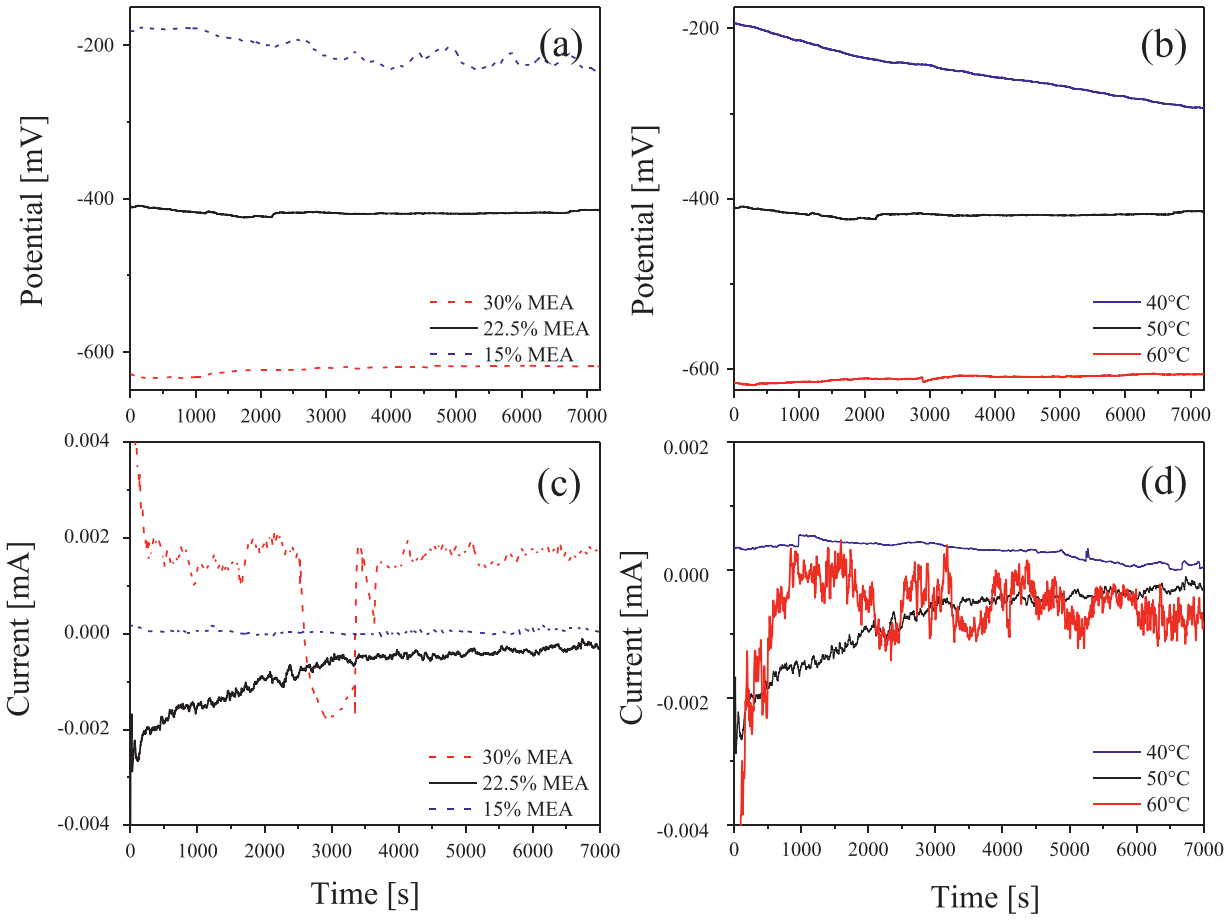

Fig. 2. Time-series obtained from corrosion process of A36 carbon steel. Potential time-series a) at 50 °C with variation of MEA concentration and b) 22.5% MEA with temperature variations. Current time series, c) at 50 °C with variation of MEA concentration and d) 22.5% MEA with temperature variations.

micrographs. Their results showed that regardless of MEA concentration, the increase in temperature increases the rate of corrosion. So, the global impact that each variable can has on the material exposed to the corrosive agent depends on the combination of multiple factors.

In general, the analysis of corrosion is carried out using different experimental methodologies, among which electrochemical techniques stand out. However, to implement such techniques it is required to include an external disturbance to the evaluated process. Additionally, one of the disadvantages is the complexity of the data interpretation due they depend on a graphic analysis and its correlation with previous works reported. An alternative is the analysis of electrochemical noise (EN) since it is easy to monitor and no disturbances to the system are required. Electrochemical noise signals are represented as small variations in potential and current, due to the interactions of the inherent electrochemical phenomena involved in the corrosion process [7,8]. The traditional analysis of EN signals is based on descriptive statistics to determine the type and degree of corrosion [9–12]. On the other hand, methodologies based on multiscale analysis provide a statistical parameter calculated from time-series (EN signals) at different time scales, which can capture the effect of the different phenomena present in the corrosion process. Amaya et al. [13] applied the multifractal analysis to the EN time-series generated during surface

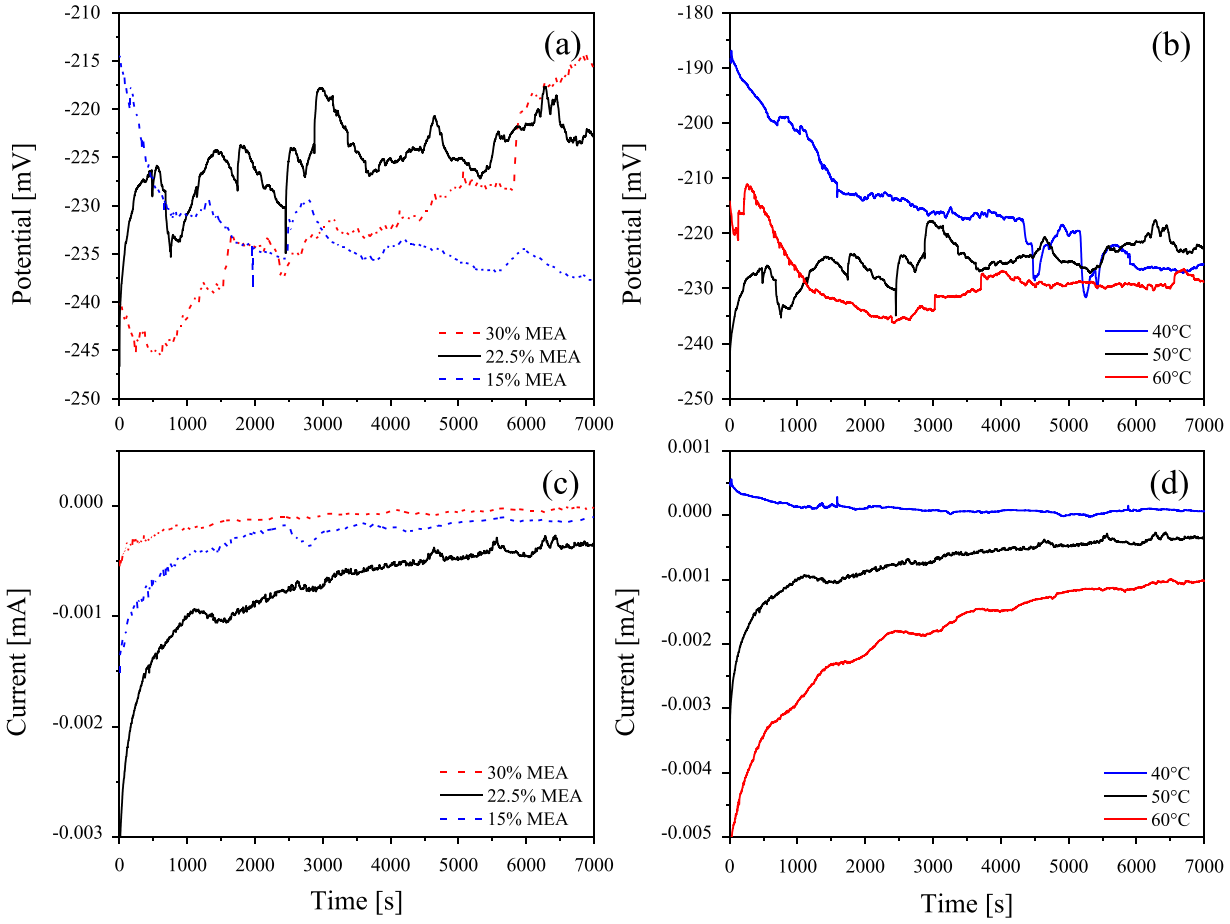

Fig. 3. Time-series obtained from corrosion process of AISI stainless steel. Potential time-series a) at 50 °C with variation of MEA concentration and b) 22.5% MEA with temperature variations. Current time series, c) at 50 °C with variation of MEA concentration and d) 22.5% MEA with temperature variations.

corrosion by a bacterial sulfate-reducing consortium, which allows them to identify complex structures on the surface of the exposed material and define a metric to quantify the degree of corrosion. Liu et al. [14] defined a fractal index from the wavelet transform to determine the degree of corrosion in a 7075-aluminum alloy with a 3.5% NaCl solution. The application of the methodologies based on the multiscale analysis allowed identifying patterns in the time series that can describe the corrosion process of different types of steels exposed to corrosive agents [15–19]. In addition, the application of multiscale time-series analysis is easy to implement and low cost. Despite this, to date it has not been applied in the study of steel corrosion in the CO_2 capture process with aqueous MEA solutions. For this reason, in this work a study is presented to determine the potential use of multiscale analysis for the corrosion evaluation in two types of steels typically used in reactive CO_2 absorption equipment (A36 carbon steel and AISI 304 stainless steel). To simulate the conditions of the absorption process, the steels were exposed in aqueous MEA solutions with CO_2, and different conditions of temperature and MEA concentration were evaluated. Potential and current time-series were collected, which were analyzed using fractal and multifractal analysis methodologies. The results show that the calculated multiscale indices can be used as indicators of type and degree of corrosion, so it could be used as a complementary tool for the diagnosis of corrosion in the CO_2 absorption process.

This paper is organized as follows. In Section 2, experimental set-up and operating conditions are described. The traditional and proposed multiscale analysis methods are also outlined in Section 2. In Section 3, results on corrosion evaluation of A36 steel and AISI 304 stainless steel exposed to aqueous monoethanolamide solutions in CO_2 capture is presented and discussed. Finally, conclusions are described in Section 4.

2. Materials and methods

2.1. Experimental set-up

The materials studied in the present study as working electrodes were A36 carbon steel and AISI 304 stainless steel, since these materials are the most used in the construction of absorption columns to CO_2 capture with amines as a solvent [3,20]. Samples of each 1 cm^2 steel were used and prior to each measurement, the samples were prepared applying a chemical cleaning according to standard ASTM G102–89 [21] with the aim of remove the corrosion products from the surface, then each sample was subjected to mechanical cleaning with silicon carbide paper and finally they were degreased with acetone and rinsed with distilled water. The corrosive environment used in electrochemical tests was an aqueous MEA-CO_2 solution. The experimental conditions were carried out in a temperature range of 40–60 °C with aqueous MEA solutions of 15–30% in weight. CO_2 was bubbled at a rate of 0.3 $m^3\ h^{-1}$, keeping the temperature constant at 4 °C, until to get a constant pH=9 (CO_2 load 0.20 mol/mol) [22].

The noise technique was carried out using a potentiostat/galvanostat from ACM instruments, calibrated according to ASTM G59–97 [23]. An electrochemical cell with a three-electrode arrangement where the working electrodes were the A36 carbon steel and AISI 304 stainless steel, adjusting the electrochemical

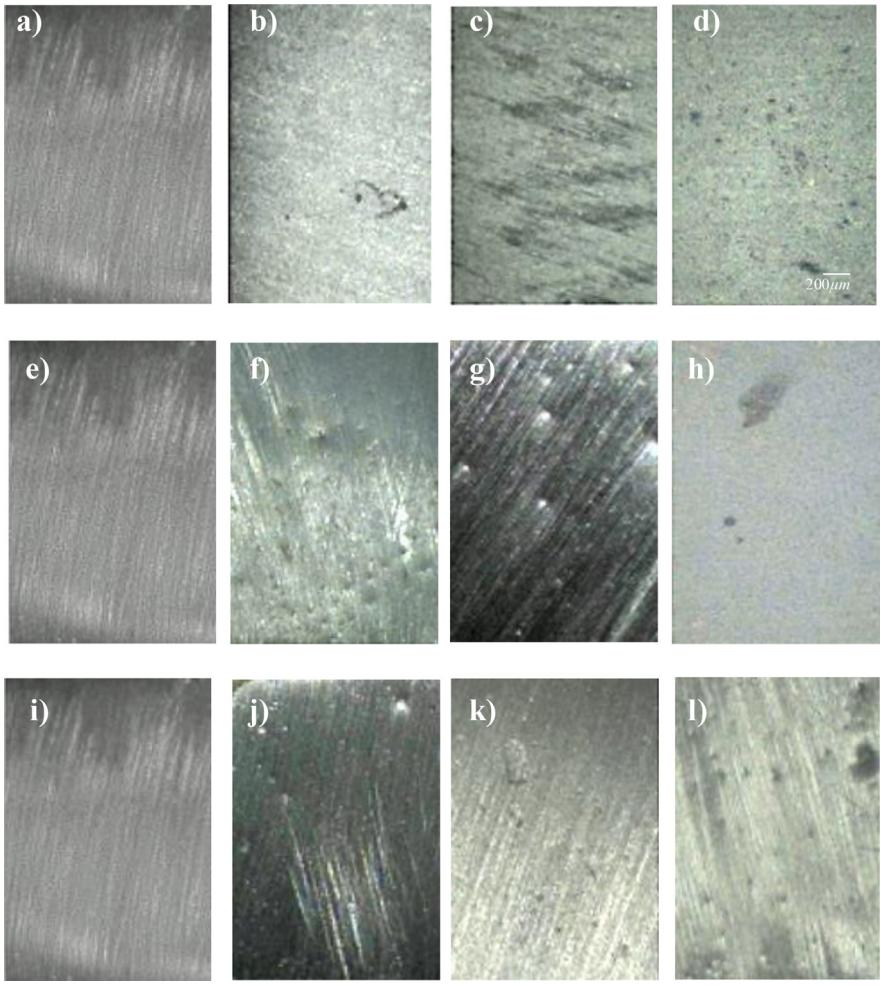

Fig. 4. Micrograph sequence of A36 steel for temperature at 40 °C, 50 °C and 60 °C: (a)-(d) 30% MEA, (e)-(h) 22% MEA, and (i)-(l) 15% MEA.

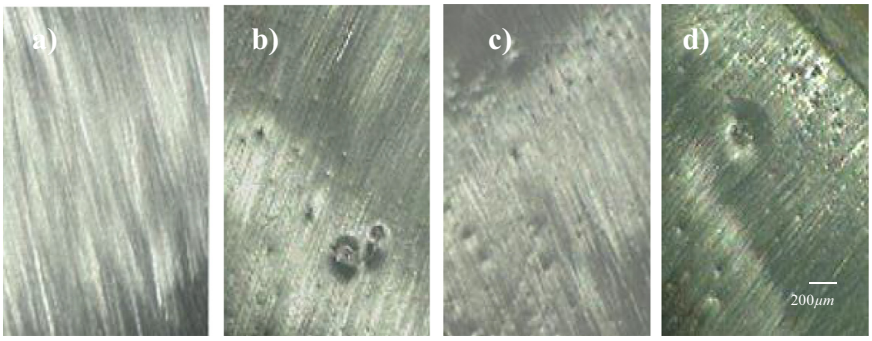

Fig. 5. (a)-(d) Micrograph sequence of AISI-304 stainless steel for temperature at 40 °C, 50 °C and 60 °C using a concentration of 22.5% MEA.

technique to the ASTM G199 [24] standard. An Ag/AgCl electrode was used as the reference electrode. The corrosion potential as a function of time was recorded during two hours of exposure of the working electrodes immersed in the electrolyte. At the beginning and end of the electrochemical noise technique, micrographs were taken of the surface of the working electrodes to observe the damage caused by the corrosion process. The images were captured in a ZEISS stemi 305 microscope with a 5: 1 zoom with an integrated 1.2 megapixels digital camera connected to a PC (DELL Inspiron 15 with 8GB RAM memory core i7 inside processor). The RGB images obtained have a size of 1920 × 2560 pixels (24.82 Mbit) with a ratio of 11.18 µm / pixel. The complete experimental set-up is shown in Fig. 1.

For the measurement of electrochemical noise, a saturated Ag/AgCl reference electrode and two nominally identical samples of A36 carbon steel and AISI 304 stainless steel were used. The equipment was calibrated according to ASTM G59–97 [23]. Current and potential time-series were captured every second for two hours (time that each experiment lasts), obtaining series of 7200 data.

2.2. Corrosion rate

Corrosion rate (V_{corr}) allows to quantify the weight loss experienced by the steels in contact with the corrosive medium from the

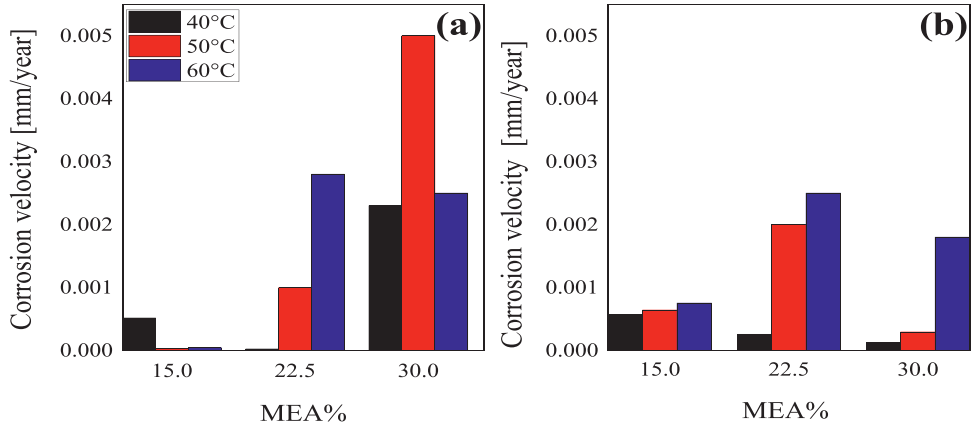

Fig. 6. Corrosion velocity, a) A36 steel and b) AISI-304 stainless steel.

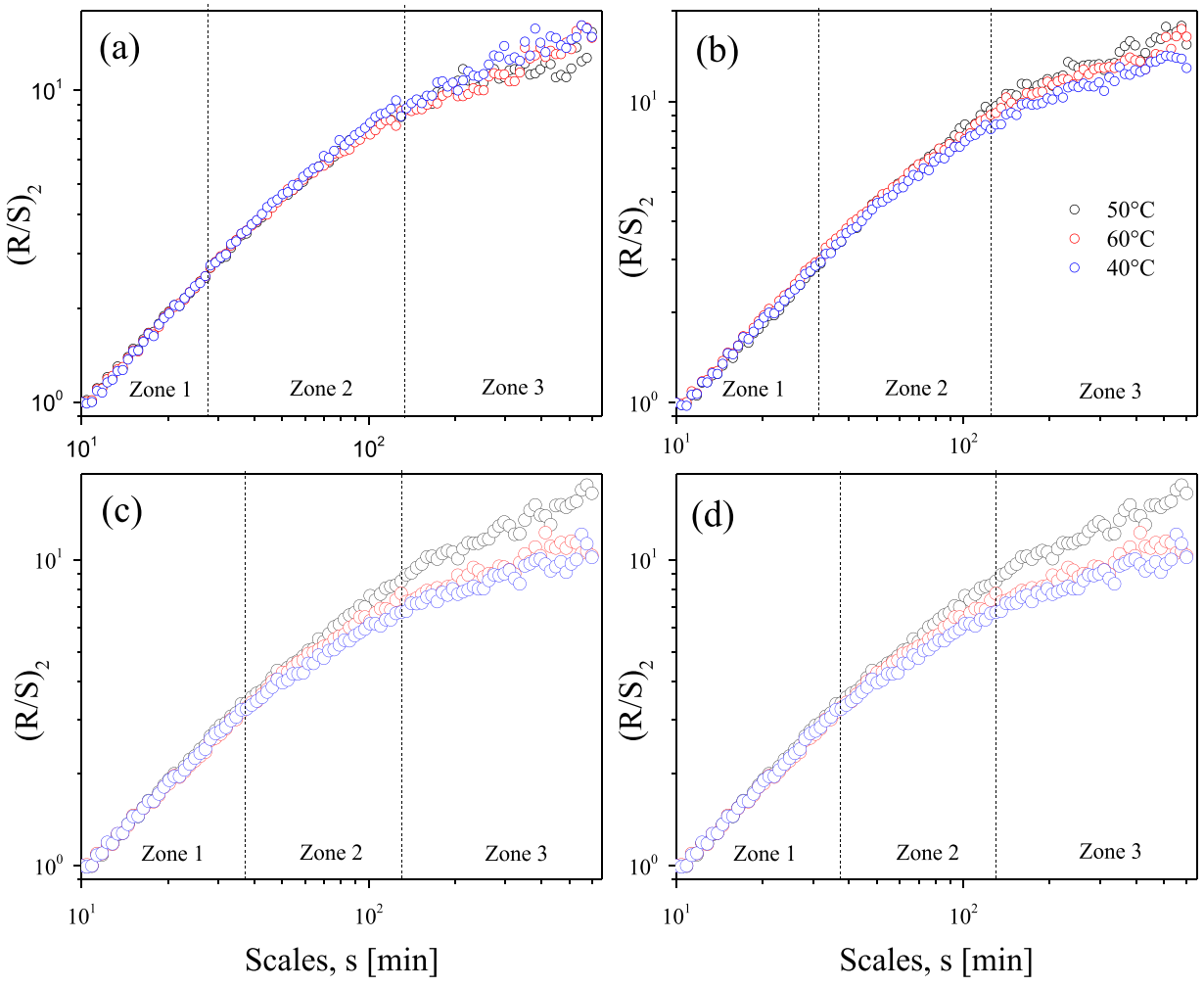

Fig. 7. R/S analysis of potential and current time-series obtained at 30% MEA and the three temperature values, a-b) A36 steel and c-d) AISI-304 stainless steel.

potential and current time-series and is calculated as,

$$V_{corr} = kEW\frac{i_{corr}}{\rho} \tag{1}$$

where k is a constant of proportionality ($k = 0.1288$, g mm year^{-1} μA^{-1} cm^{-1}), ρ is the density of the metal or alloy used (g cm^{-3}) and EW is the equivalent weight of the metal or alloy used [21]. i_{corr} is the current density (μA cm^{-2}), which is calculated as

$$i_{corr} = \frac{B}{R_n} \tag{2}$$

where B represents the Stern-Geary constant that can take the values of 26 mV and 52 mV depending on the type of material analyzed and R_n is the noise resistance calculated with standard deviation of the potential and current series, $R_n = \frac{\sigma_v}{\sigma_I}$ [25].

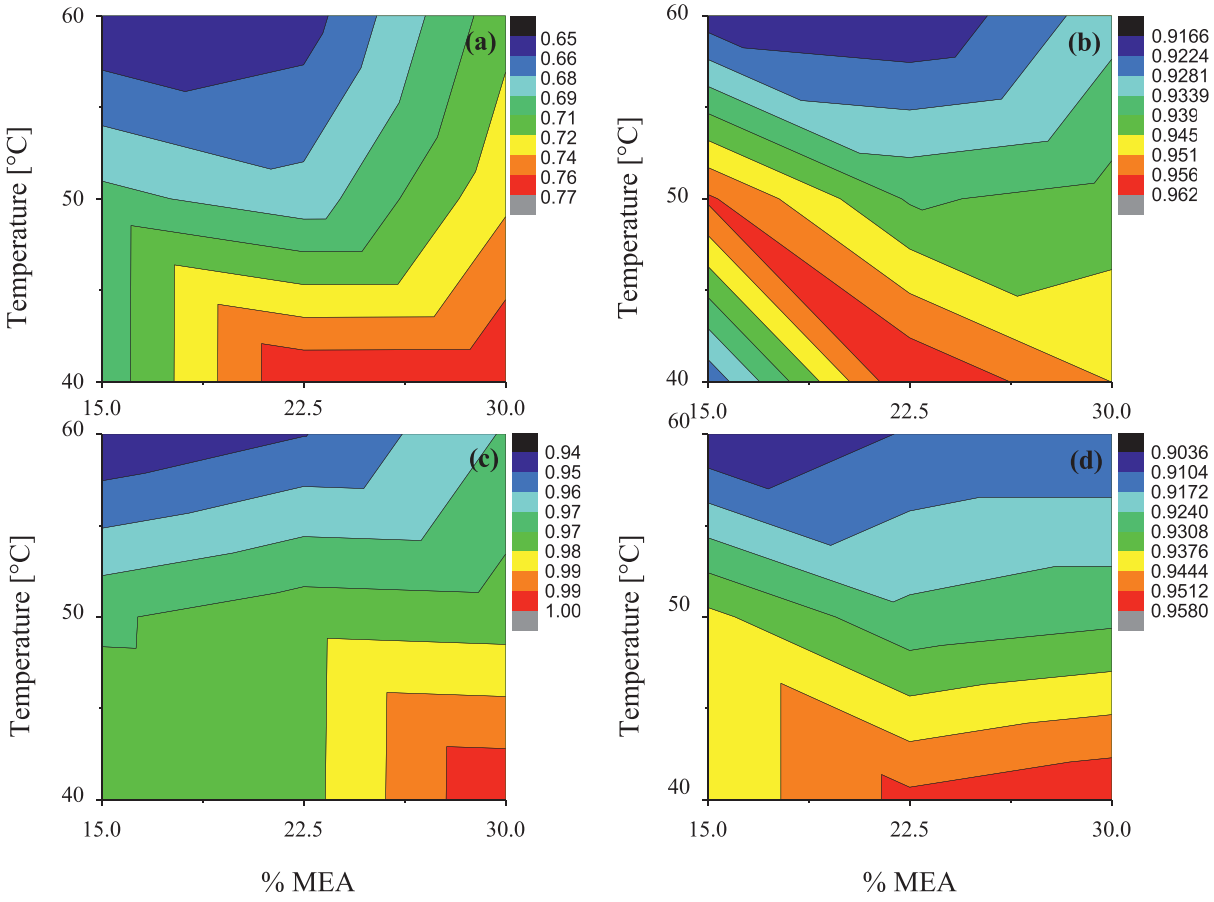

Fig. 8. Hurst exponent of the first zone, a-b) A36 steel and c-d) AISI-304 stainless steel.

2.3. R/S analysis

R/S analysis is a statistical test used to quantify the dynamics of time series and to determine the existence of fractal characteristics in a physical process [26-28]. The R/S statistical measures the range of the deviations of the partial sums in a time series about its average, rescaled by the series standard deviation. For a time-series X with length N, it is considered a subsequence Y_{NS} of length N_S, where $N_S<N$. The R/S statistics is calculated as

$$(R/S)_2 = \frac{1}{\sigma_{Ns}}\left[\max_{1\le k\le Ns}\left\{\sum_{i=1}^{k}(y_i-\bar{y}_{N_S})\right\}-\min_{1\le k\le Ns}\left\{\sum_{i=1}^{k}(y_i-\bar{y}_{N_S})\right\}\right] \tag{3}$$

where $\bar{y}_{N_S}=\frac{1}{N_S}\sum_{i=1}^{Ns}y_i$ is subsequence mean and $\sigma_{Ns}=\left[\frac{1}{N_S}\sum_{k=1}^{N_S}(y_k-\bar{y}_{N_S})^2\right]^{1/2}$ is the sample standard deviation. The R/S statistic follows a power law, $(R/S)=aN_S^H$ where a is a constant and H is the Hurst exponent. A log-log plot of (R/S) as a function of $N_S\in(N_{S,\min},N_{S,\max})$, gives a straight line with slope H. If the series data is independent (e.g., white-noise process), the plot is roughly a straight line with slope $H=0.5$. If $H>0.5$, the time series is persistent, indicating the presence of long-term auto-correlations. Conversely, if $H<0.5$ auto-correlations in the signal are anti-persistent [29,30].

2.3.1. Multifractal analysis

As well known, multifractality is a useful tool for explaining many patterns seen in nature. Particularly, multifractal analysis allows to investigate a mixture of fractal dimensions characterize the inherent complexity in some data series. Based on the thoughts of Barabasi and Vicsek [31], and Katsuragi and Honjo [32], the multifractal analysis can be done through the calculation of the rescaled range by means of the q-moment of σ_s, that is,

$$\sigma_{Ns,q}=\left[\frac{1}{N_S}\sum_{k=1}^{Ns}(y_k-\bar{y}_{Ns})^q\right]^{\frac{1}{q}} \tag{4}$$

In this case, the R/S statistical is given by $(R/S)_q=\frac{\sigma_{Ns}}{\sigma_{Ns,q}}(R/S)_2$, and the average range is expected to follow the scaling behavior $(R/S)_q=as^{2H_q}$, where H_q is the q-th Hurst exponent. If H_q is constant for all q then the underlying time-series is monofractal. A non-trivial dependence of H_q on q indicates that the process is multifractal. It should be recalled that a multifractal system is a generalization of a fractal system in which a single exponent (the fractal dimension) is not enough to describe its dynamics. In general, multifractality also indicates the nonlinear nature of the mechanisms that generated the series [13,16,19]. To describe the degree of multifractality, a multifractality index is defined as,

$$I_M=\max(H(q))-\min(H(q)) \tag{7}$$

where $H(q)$ is the H value as a function of q.

3. Results and discussion

Fig. 2 shows the potential and current time-series of A36 carbon steel obtained by different experimental conditions of temperature and MEA concentrations. In Fig. 2a-b is observed that in the larger temperature values and MEA concentration, the potential measurements become more negative, which suggests that there is

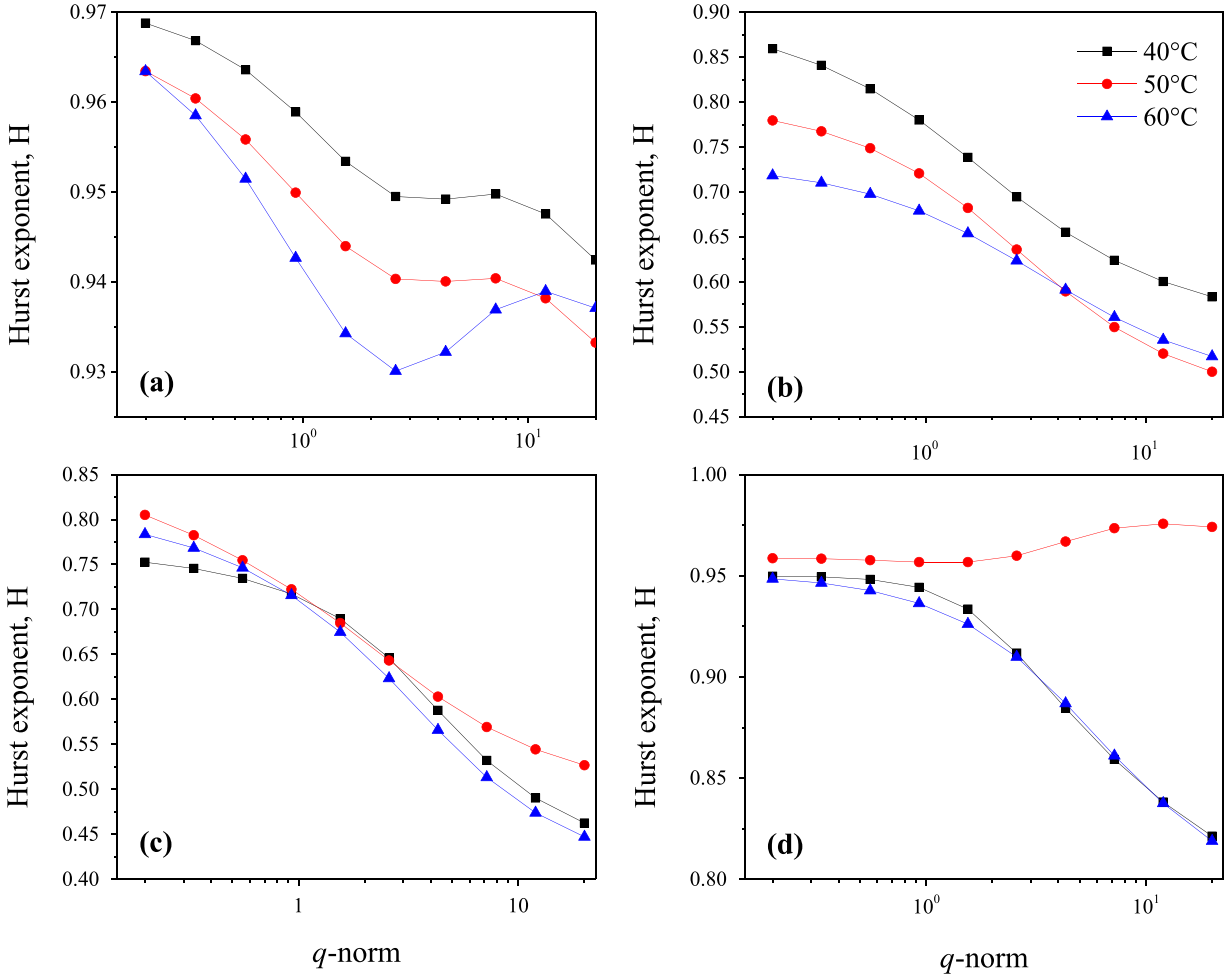

Fig. 9. Hurst exponent as a function of the q-norm of the potential series obtained at 30% and 15% MEA for the three temperature values, a-b) A36 steel and c-d) AISI-304 stainless steel.

a greater effect of corrosion in the steel [33]. Fig. 3 shows the potential and current series for AISI 304 stainless steel, where greater fluctuations are observed than in those observed in A36 carbon steel. Likewise, for both effects (temperature and MEA concentration) the potential values remain in the range of 100–200 mV (Fig. 3a-b), which suggests the formation of a thin passive layer of chromium oxide in stainless steel [34].

Fig. 4 shows micrographs of A36 carbon steel exposed to MEA solutions at 40, 50 and 60 °C. For MEA at 30% (Figs. 4a-d) it is observed that as the temperature increases the damage to the metal is more visible, at 50 °C a homogeneous damage can be seen, while at 60 °C damage by pitting is observed. Considering MEA at 22.5% (Figs. 4e-h) it is observed that at 40 °C the formation of a protective layer that prevents corrosion occurs. Finally, for MEA solution at 15%, temperature changes show no apparent damage to the steel surface. In general, it is observed that carbon steel exhibits greater corrosion effects with increasing temperature and MEA concentration, which corresponds to that reported by Kittel et al. [3] and Li et al. [20]. On the other hand, AISI 304 steel micrographs do not reflect considerable damage on the metal surface, but the formation of a layer is observed that promotes the inhibition of the corrosion process. It is inferred that the layer formed is made of chromium oxide that increases its thickness as time increases, reducing the damage of the steel due to corrosion. In Fig. 5 is showed the micrograph sequence for temperature at 40 °C, 50 °C and 60 °C using a concentration of 22.5% MEA.

Corrosion rate allows estimating the weight loss experienced by the steel samples exposed in the MEA-CO_2 solution. Fig. 6 shows the V_{corr} calculated for changes in temperature and MEA concentration, where it is observed that V_{corr} of A36 carbon steel is greater (0.005 mm year^{-1}) than that of stainless steel (0.0025 mm year^{-1}) and it agrees with what was reported by Kittel et al. [3]. Note that, for stainless steel, the increase in V_{corr} is directly related to temperature, while in carbon steel a higher MEA concentration produce a higher the corrosion rate. The characteristics of AISI-304 provide greater stability and resistance, making it more suitable for conditions to which the CO_2 absorption process is carried out [20].

Considering potential and current time-series obtained for MEA at 30% and for all the temperature values, Fig. 7 shows the R/S statistic as a function of the scale s, where it is observed that the behavior does not follow a single power law, noting a change in slope of the R/S statistic in the entire range of scales considered (s_{min} to s_{max}). For all the evaluated experiments, three important slope changes can be identified, which are denoted as zones 1, 2 and 3, and a value of the Hurst exponent is calculated for each zone. The existence of more than one scaling exponent is indicative that the fluctuations in both time series (potential and current) can identify three phenomena at different time scales. These results are consistent with those found in steels under different conditions of the corrosive agent [16–19].

The H values are shown in Table 1, where the Hurst exponents change according to the temperature and MEA concentration conditions used. For example, keeping the MEA concentration con-

Table 1
Hurst exponent calculated using the potential time-series for A36 carbon steel.

MEA concentration (%)	Zone 1			Zone 2			Zone 3		
	Temperature [°C]								
	40	50	60	40	50	60	40	50	60
30	0.972	0.997	0.991	0.777	0.742	0.724	0.484	0.416	0.432
22.5	0.977	0.975	0.954	0.777	0.689	0.659	0.457	0.393	0.342
15	0.978	0.970	0.924	0.704	0.703	0.651	0.439	0.400	0.337

stant, the value of H in zone 1 decreases with increasing temperature. For the two steels, Fig. 8 shows a color graph of the H values at the different experimental conditions. Fig. 8a shows that at 30% MEA and $T = 60$ °C the maximum value is reached, which coincides with the conditions where the greatest oxidation of carbon steel is promoted. While at conditions of 15% MEA and $T = 60$ °C, the lowest H values are presented and are associated with the formation of the layer that reduces the effect of corrosion. Such effect is corroborated with that observed in Fig. 4 and corresponds with that reported by different authors [35–37]. The R/S analysis of the potential and current series of AISI-304 stainless steel obtained similar results to carbon steel. The results generated from the potential series are shown in Fig. 8b, where it is observed that the highest value of H is associated with the greatest effect of corrosion on AISI-304 steel (30% MEA and $T = 40$ °C).

Multifractal analysis of the potential and current time-series was performed, finding that for both cases the Hurst exponent exhibits a non-linear behavior for variations of the q-norm, which suggests that the corrosion process cannot be represented by a structure monofractal (Fig. 9). Multifractality is associated with the complexity of the process, due to the interaction of multiple physicochemical phenomena, such as birth, growth of corroded sites, passivation, rupture of the passive layer, repassivation, etc., which can be associated with the degree of corrosion of stainless steel exposed to different corrosive agents [13,14,18,19]. Fig. 10 shows IM calculated with the potential time-series of AISI 304 stainless steel for all conditions of the temperature and MEA concentration evaluated, finding that the smallest values of the IM correspond to the conditions where the corrosion exhibits greater damage to the metal. These results correspond to that observed in the micrographs, correctly identifying the areas that the Hurst exponent cannot identify. For example, at 40 °C whereas MEA concentration decreases the effect of corrosion is also reduced, which is not observed at concentrations of 22.5 and 15% MEA. For carbon steel, Fig. 10b shows the IM at different temperature and MEA concentration conditions, observing that IM increases with respect to temperature and decreases with a change in MEA concentration. This behavior is like that obtained with the Hurst exponent and to the physical changes in the steel observed in the micrographs.

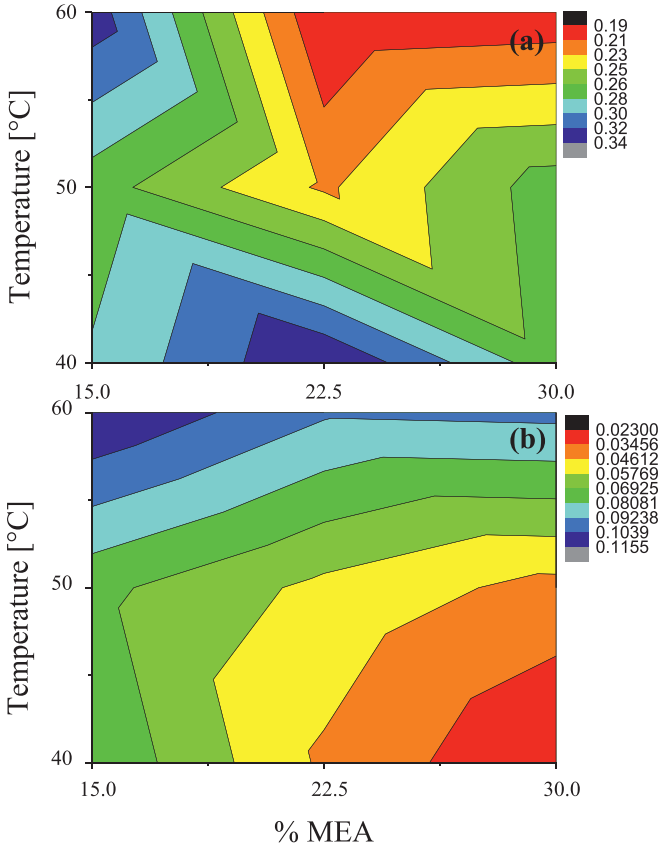

Fig. 10. Multifractal index, a) A36 steel and b) AISI-304 stainless steel.

4. Conclusions

A multiscale analysis of time-series for the evaluation of the corrosion of A36 carbon steel and AISI-304 stainless steel exposed to aqueous solutions of monoethanolamine (MEA) with CO_2, was developed to evaluate the scope of the proposed methodology, experiments were carried out at different temperature conditions and amine concentrations, finding that the temperature has a direct effect with the corrosive process of carbon steel A36, while in AISI-304 stainless steel it is promoted the formation of a protective layer, which inhibits corrosion. MEA concentration shows less effect and it was found that at low MEA concentrations (i.e. 15% MEA) the formation of a passive layer is generated, which reduces the oxidation of the steel. For both steels, multiscale parameters can identify the formation of layers that inhibit the damage to the metal by the corrosion at different conditions of temperature and MEA concentration. The multifractal index shows a better correlation of the oxidative behavior, since it clearly shows the conditions in which corrosion is promoted and/or inhibited in both steels. Finally, multiscale analysis could be used as a complementary tool for the diagnosis of corrosion in CO_2 absorption columns.

Declaration of Competing Interest

The authors declare that they have no known competing financial interests or personal relationships that could have appeared to influence the work reported in this paper.

CRediT authorship contribution statement

Mariana Ramírez-Platas: Formal analysis, Methodology. **Miguel A. Morales-Cabrera:** Writing – original draft. **Victor M. Rivera:** Visualization. **Epifanio Morales-Zarate:** Writing – review & editing. **Eliseo Hernandez-Martinez:** Conceptualization, Supervision.

References

[1] Idem R, Wilson M, Tontiwachwuthikul P, Chakma A, Veawab A, Aroonwilas A, Gelowitz D. Pilot plant studies of the CO_2 capture performance of aqueous MEA and mixed MEA/MDEA solvents at the University of Regina CO_2 capture technology development plant and the boundary dam CO_2 capture demonstration plant. Ind Eng Chem Res 2006;45(8):2414–20. doi:10.1021/ie050569e.

[2] Luis P. Use of monoethanolamine (MEA) for CO_2 capture in a global scenario: consequences and alternatives. Desalination 2016;380:93–9. doi:10.1016/j.desal.2015.08.004.

[3] Kittel J, Idem R, Gelowitz D, Tontiwachwuthikul P, Parrain G, Bonneau A. Corrosion in MEA units for CO_2 capture: pilot plant studies. Energy Procedia 2009;1(1):791–7. doi:10.1016/j.desal.2015.08.004.

[4] Kittel J, Fleury E, Vuillemin B, Gonzalez S, Ropital F, Oltra R. Corrosion in alkanolamine used for acid gas removal: from natural gas processing to CO_2 capture. Mater Corros 2012;63:223–30. doi:10.1002/maco.201005847.

[5] Xiang Y, Yan M, Choi YS, Young D, Nesic S. Time-dependent electrochemical behavior of carbon steel in MEA-based CO_2 capture process. Int J Greenh Gas Con 2014;30:125–32. doi:10.1016/j.ijggc.2014.09.003.

[6] Erfani A, Boroojerdi S, Dehghani A, Yarandi M. Investigation of carbon steel and stainless-steel corrosion in a MEA based CO_2 removal plant. Pet Coal 2015;57(1):48–55. https://www.vurup.sk/wp-content/uploads/dlm_uploads/2017/07/pc_1_2015_boroojerdi_320_kor2.pdf.

[7] Cottis RA. Interpretation of electrochemical noise data. Corrosion 2001;57(3):265–85. doi:10.5006/1.3290350.

[8] Xia DH, Song SZ, Behnamian Y. Detection of corrosion degradation using electrochemical noise (EN): review of signal processing methods for identifying corrosion forms. Corros Eng Sci Techn 2016;51(7):527–44. doi:10.1179/1743278215Y.0000000057.

[9] Legat A, Dolecek V. Corrosion monitoring system based on measurement and analysis of electrochemical noise. Corrosion 1995;51(4):295–300. doi:10.5006/1.3293594.

[10] Kearns JR, Scully JR, Roberge PR, Reichert DL, Dawson JL. Electrochemical noise measurement for corrosion applications. West Conshohocken, USA: ASTM International; 1996.

[11] Al-Mazeedi HAA, Cottis RA. A practical evaluation of electrochemical noise parameters as indicators of corrosion type. Electrochim Acta 2004;49:2787–93. doi:10.1016/j.electacta.2004.01.040.

[12] Hou Y, Aldrich C, Lepkova K, Machuca LL, Kinsella B. Monitoring of carbon steel corrosion by use of electrochemical noise and recurrence quantification analysis. Corros Sci 2016;112:63–72. doi:10.1016/j.corsci.2016.07.009.

[13] Amaya M, Sosa E, Romero JM, Alvarez-Ramirez J, Meraz M, Puebla H. Multifractality in an electrochemical noise signal by a biocorrosion system. Fractals 2004;12(03):347–54. doi:10.1142/S0218348X04002598.

[14] Liu XF, Wang HG, Gu HC. Fractal characteristic analysis of electrochemical noise with wavelet transform. Corros Sci 2006;8(6):1337–67. doi:10.1016/j.corsci.2005.06.001.

[15] Planinšič P, Petek A. Characterization of corrosion processes by current noise wavelet-based fractal and correlation analysis. Electrochim Acta 2008;53(16):5206–14. doi:10.1016/j.electacta.2008.02.051.

[16] Xu Y, Qian C, Pan L, Wang B, Lou C. Comparing monofractal and multifractal analysis of corrosion damage evolution in reinforcing bars. PLoS ONE 2012;7(1):e29956. doi:10.1371/journal.pone.0029956.

[17] Wang Q, Wang Y, He M, Ni Z, Wang Q, Bao H, Li X, Yang W, Tao X. Experimental and fractal studies on corrosion inhibition performance of Ophiopogon japonicus leaf extract on carbon steel in HCl. Mater Res Express 2019;6(10):1065e6. https://iopscience.iop.org/article/10.1088/2053-1591/ab4107/pdf.

[18] López JL, Veleva L, López-Sauri DA. Multifractal detrended analysis of the corrosion potential fluctuations during copper patina formation on Its first stages in sea water. Int J Electrochem Sci 2014;9:1637–49. http://www.electrochemsci.org/papers/vol9/90401637.pdf.

[19] Sanchez-Ortiz W, Andrade-Gómez C, Hernandez-Martinez E, Puebla H. Multifractal Hurst analysis for identification of corrosion type in AISI 304 stainless steel. Int J Electrochem Sci 2015;10:1054–64. http://www.electrochemsci.org/papers/vol10/100201054.pdf.

[20] Li W, Landon J, Irvin B, Zheng L, Ruh K, Kong L, Nikolic H. Use of carbon steel for construction of post-combustion CO_2 capture facilities: a pilot-scale corrosion study. Ind Eng Chem Res 2017;56(16):4792–803. doi:10.1021/acs.iecr.7b00697.

[21] ASTM G102-89 Standard practice for calculation of corrosion rates and related information from electrochemical measurements. West Conshohocken: ASTM International; 2004.

[22] Soosaiprakasam IR, Veawab A. Corrosion and polarization behavior of carbon steel in MEA-based CO2 capture process. Int J Greenh Gas Control 2008;2(4):553–62. doi:10.1016/j.ijggc.2008.02.009.

[23] ASTM G59-97 Standard test method for conducting potentiodynamic polarization resistance measurements. West Conshohocken: ASTM International; 2014.

[24] ASTM G-199 Standard guide for electrochemical noise measurement. West Conshohocken: ASTM International; 2009.

[25] Tan YJ. Interpreting electrochemical noise resistance as a statistical linear polarization resistance. J Corros Sci Eng 1999;1:1. -1 http://hdl.handle.net/10536/DRO/DU:30048004 .

[26] Méndez-Acosta HO, Hernandez-Martinez E, Jáuregui-Jáuregui JA, Alvarez-Ramirez J, Puebla H. Monitoring anaerobic sequential batch reactors via fractal analysis of pH time series. Biotechnol Bioeng 2013;110(8):2131–9. doi:10.1002/bit.24838.

[27] Gabriel-Guzmán M, Rivera VM, Cocotle-Ronzón Y, García-Díaz S, Hernandez-Martinez E. Fractality in coffee bean surface for roasting process. Chaos Soliton Fract 2017;99:79–84. doi:10.1016/j.chaos.2017.03.056.

[28] Yadav R, Agarwal DC, Kumar M, Rajput P, Tomar DS, Pandey SN, Mittal AK. Effect of angle of deposition on the fractal properties of ZnO thin film surface. Appl Surf Sci 2017;416:51–8. doi:10.1016/j.apsusc.2017.04.098.

[29] Hurst HE. Long-term storage capacity of reservoirs. Trans Ame Soc Civ Eng 1951;116:770.

[30] Mandelbrot BB, Wallis JR. Computers experiments with fractional Gaussian noises. Part 1: sample graphs, averages and variances. Water Resour Res 1969;5:228–41. doi:10.1029/WR005i001p00228.

[31] Barabási AL, Vicsek T. Multifractality of self-affine fractals. Phys Rev A 1991;44(4):2730. doi:10.1103/PhysRevA.44.2730.

[32] Katsuragi H, Honjo H. Multiaffinity and entropy spectrum of self-affine fractal profiles. Phys Rev E 1999;59(1):254. doi:10.1103/PhysRevE.59.254.

[33] Power GP, Ritchie IM. Mixed potential measurements in the elucidation of corrosion mechanisms-1. Introductory theory. Electrochim Acta 1981;26(8):1073–8. doi:10.1016/0013-4686(81)85079-7.

[34] Estupiñán F, Tristancho JL, Almeraya F. Análisis de los transitorios en ruido electroquímico para aceros inoxidables que presentan corrosión por picaduras. Sci et Technica 2010;17(46):34–9. doi:10.22517/23447214.1155.

[35] Fytianosa G, Grimstvedtb A, Knuutilaa H, Svendsena HF. Effect of MEA's degradation products on corrosion at CO_2 capture plants. Energy Procedia 2014;63:1869–75. doi:10.1016/j.egypro.2014.11.195.

[36] Benamor A, Al-Marri MJ. Modeling analysis of corrosion behavior of carbon steel in CO_2 loaded amine solutions. Int J Chem Eng Appl 2014;5(4):353. doi:10.7763/IJCEA.2014.V5.408.

[37] Gunasekaran P, Veawab A, Aroonwilas A. Corrosivity of amine-based absorbents for CO_2 capture. Energy Procedia 2017;114:2047–54. doi:10.1016/j.egypro.2017.03.1339.